Since January 2020 Elsevier has created a COVID-19 resource centre with free information in English and Mandarin on the novel coronavirus COVID-19. The COVID-19 resource centre is hosted on Elsevier Connect, the company's public news and information website.

Ecological Complexity 47 (2021) 100941

Contents lists available at ScienceDirect

Ecological Complexity

journal homepage: www.elsevier.com/locate/ecocom

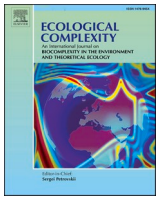

Original research article

The co-circulation of two infectious diseases and the impact of vaccination against one of them

G.F. Puga [a], L.H.A. Monteiro [a,b,*]

[a] Universidade Presbiteriana Mackenzie, PPGEEC, São Paulo, SP, Brazil
[b] Universidade de São Paulo, Escola Politécnica, São Paulo, SP, Brazil

ARTICLE INFO

Keywords:
Co-circulating infections
COVID-19
Immunosuppression
Measles
Probabilistic cellular automaton
Vaccination

ABSTRACT

An epidemiological model based on probabilistic cellular automaton is proposed to investigate the dynamics of two co-circulating infections. In the model, one of these two diseases compromises the immune response to future infections; however, there is vaccine against this immunosuppressive disease. The goal is to evaluate the impact of the vaccination coverage on the prevalence and on the cumulative deaths associated with both contagious diseases. The performed numerical simulations highlight the importance of vaccination on decreasing morbidity and mortality. The results are discussed from a public health standpoint, by taking into account outbreaks of measles and COVID-19.

1. Introduction

There are about 1400 species of infectious agents that are pathogenic to humans (Woolhouse and Gowtage-Sequeria, 2005) and it is not uncommon to find some of them simultaneously infecting a community. Hence, there are several theoretical models about co-circulating pathogens. These models are usually written in terms of ordinary differential equations. For instance, there are works about the interaction between dengue and leptospirosis (Alemneh, 2020), pneumonia and meningitis (Tilahun, 2019), HIV and hepatitis C (Moualeu et al., 2011), two strains of influenza (Zhang et al., 2013), two strains of dengue (Anggriani et al., 2019).

The co-circulation of infections can be viewed as a complex system, due to the usual large number of variables and parameters composing the corresponding epidemic model. Here, a model with 10 variables and 20 parameters is proposed to study the dynamics of two co-circulating infections. This model is based on probabilistic cellular automaton (PCA), an approach that has been used in several works on ecological and/or epidemiological systems (Ahmed et al., 1998; Boccara et al., 1994; Doran and Laffan, 2005; Ferreri and Venturino, 2013; Nagatani and Tainaka, 2018; Sfa et al., 2020; Slimi et al., 2009).

In this work, disease-1 causes immunosuppression, which impairs the immune response to a subsequent disease-2 infection; however, vaccine against disease-1 is available. The main aim here is to investigate the impact of vaccination against disease-1 on the prevalence and on the cumulative deaths related to both diseases.

This manuscript is organized as follows. In Section 2, the PCA model is introduced. In Section 3, results from computational simulations are presented. In Section 4, these results are discussed by considering measles and COVID-19 as immunity-damaging diseases.

2. The PCA epidemic model

Assume that each cell of a two-dimensional lattice $n \times n$ corresponds to an individual of the host population. The boundary condition of this lattice is taken as periodic, which means that the left and right edges are connected and the top and bottom edges are connected too; therefore, each individual is equivalent from a geographical point of view. Assume also that each individual is socially connected to the eight surrounding neighbors; that is, the interactions among the individuals occurs within a Moore neighborhood of unit radius (Wolfram, 1994).

In this population, there occurs the co-circulation of two contagious diseases, called disease-1 and disease-2. Assume that, at each time step t, each individual is in one of the following ten health states:

- S: susceptible to both diseases;
- V: vaccinated against disease-1; susceptible to disease-2;
- I_1: infected by disease-1, susceptible to disease-2;
- I_2: infected by disease-2, susceptible to disease-1;
- I_{12}: infected by disease-1, recovered from disease-2;

* Corresponding author.
E-mail addresses: luizm@mackenzie.br, luizm@usp.br (L.H.A. Monteiro).

https://doi.org/10.1016/j.ecocom.2021.100941
Received 23 January 2021; Received in revised form 4 May 2021; Accepted 21 May 2021
Available online 13 June 2021

- I_{21}: infected by disease-2, recovered from disease-1;
- I: infected by disease-2, vaccinated against disease-1;
- R_1: recovered from disease-1, susceptible to disease-2;
- R_2: recovered from disease-2, susceptible to disease-1;
- R: immune to both diseases.

The state transitions are governed by 20 probabilistic rules: 5 rules governing the contagion processes; 1 rule the vaccination process; 5 the recovery processes; 9 the death processes. When infected, vaccinated, or recovered individuals die, susceptible individuals replace them. Therefore, in this population, deaths are balanced by births, so that the total number of individuals $N = n^2$ remains constant. Co-infections (simultaneous infection by both diseases) are here not considered. In addition, recovery and vaccination lead to a full long-lasting immunity.

The 5 state transitions related to the spreading of these diseases are:

$$S + I_1 + I_{12} \xrightarrow{xP_1} I_1 + I_1 + I_{12} \tag{1}$$

$$S + I_2 + I_{21} + I \xrightarrow{(1-x)P_2} I_2 + I_2 + I_{21} + I \tag{2}$$

$$R_2 + I_1 + I_{12} \xrightarrow{P_3} I_{12} + I_1 + I_{12} \tag{3}$$

$$R_1 + I_2 + I_{21} + I \xrightarrow{P_4} I_{21} + I_2 + I_{21} + I \tag{4}$$

$$V + I_2 + I_{21} + I \xrightarrow{P_5} I + I_2 + I_{21} + I \tag{5}$$

The state transitions related to vaccination against disease-1 is:

$$S \xrightarrow{\nu} V \tag{6}$$

The 5 state transitions related to recovery from these diseases are:

$$I_1 \xrightarrow{b_1} R_1 \tag{7}$$

$$I_2 \xrightarrow{b_2} R_2 \tag{8}$$

$$I_{12} \xrightarrow{\beta_1} R \tag{9}$$

$$I_{21} \xrightarrow{\beta_2} R \tag{10}$$

$$I \xrightarrow{\beta} R \tag{11}$$

The 5 state transitions related to death caused by these diseases are:

$$I_1 \xrightarrow{c_1} S \tag{12}$$

$$I_2 \xrightarrow{c_2} S \tag{13}$$

$$I_{12} \xrightarrow{\gamma_1} S \tag{14}$$

$$I_{21} \xrightarrow{\gamma_2} S \tag{15}$$

$$I \xrightarrow{\gamma} S \tag{16}$$

The 4 state transitions related to death due to other reasons are:

$$R_1 \xrightarrow{d_1} S \tag{17}$$

$$R_2 \xrightarrow{d_2} S \tag{18}$$

$$R \xrightarrow{d} S \tag{19}$$

$$V \xrightarrow{\delta} S \tag{20}$$

For S-individuals: at each time step, there are a probability xP_1 of a S-individual being infected and becoming an I_1-individual and a probability $(1-x)P_2$ of being infected and becoming an I_2-individual, with $x = (i_1 + i_{12})/(i_1 + i_{12} + i_2 + i_{21} + i)$, $P_1 = 1 - \exp[-k_1(i_1 + i_{12})]$, and $P_2 = 1 - \exp[-k_2(i_2 + i_{21} + i)]$. In these expressions, i_1, i_2, i_{12}, i_{21}, and i are the numbers of I_1, I_2, I_{12}, I_{21}, and I-individuals in the neighborhood of this S-individual, respectively. For instance, if $i_1 = 1$, $i_2 = 1$, $i_{12} = 1$, $i_{21} = 0$, and $i = 0$, then $x = 2/3$, which is the proportion of individuals with disease-1 in the neighborhood of this S-individual; obviously, $(1-x) = 1/3$ is the proportion of individuals with disease-2. Thus, the greater the number of neighbors infected by a specific disease, the greater the probability of the S-individual getting such a disease. Also, k_1 and k_2 are positive constants related to the infectiousness of disease-1 and disease-2, respectively. Note that if $i_1 + i_{12} = 0$, then $P_1 = 0$; therefore, a S-individual can get disease-1 only if there are neighbors with this disease. Consistently, if $i_2 + i_{21} + i = 0$, then $P_2 = 0$. Note that if $k_1(i_1 + i_{12}) \to \infty$, then $P_1 \to 1$; if $k_2(i_2 + i_{21} + i) \to \infty$, then $P_2 \to 1$. These infection rules correspond to Eqs. (1) and (2), and they are applied only if there is at least one infected individual in the neighborhood of this S-individual; that is, only if $i_1 + i_{12} + i_2 + i_{21} + i \neq 0$. If this S-individual is not infected either by disease-1 or by disease-2, then there is a probability ν of being vaccinated against disease-1, as stated in Eq. (6).

For I_1-individuals: at each time step, there is a probability b_1 of being cured and becoming a R_1-individual. If this I_1-individual remains sick, there is a probability c_1 of dying due to disease-1. These processes of recovery and death are represented by Eqs. (7) and (12), respectively.

For I_2-individuals: at each time step, there is a probability b_2 of being cured and becoming a R_2-individual. If this I_2-individual remains sick, there is a probability c_2 of dying due to disease-2. These processes of recovery and death are represented by Eqs. (8) and (13), respectively.

For R_2-individuals: at each time step, there is a probability $P_3 = 1 - \exp[-k_3(i_1 + i_{12})]$ of being infected by disease-1 and becoming an I_{12}-individual. In this expression, k_3 is a positive constant. If this R_2-individual was not infected, there is a probability d_2 of dying. These processes of infection and death are represented by Eqs. (3) and (18), respectively.

For R_1-individuals: at each time step, there is a probability $P_4 = 1 - \exp[-k_4(i_2 + i_{21} + i)]$ of being infected by disease-2 and becoming an I_{21}-individual. In this expression, k_4 is a positive constant. If this R_1-individual was not infected, there is a probability d_1 of dying. These processes of infection and death are represented by Eqs. (4) and (17), respectively.

For V-individuals: at each time step, there is a probability $P_5 = 1 - \exp[-k_5(i_2 + i_{21} + i)]$ of being infected by disease-2 and becoming an I-individual. In this expression, k_5 is a positive constant. If this V-individual was not infected, there is a probability δ of dying. These processes of infection and death are represented by Eqs. (5) and (20), respectively.

For I_{12}-individuals: at each time step, there is a probability β_1 of being cured and becoming a R-individual. If this I_{12}-individual remains sick, there is a probability γ_1 of dying due to disease-1. These processes of recovery and death are represented by Eqs. (9) and (14), respectively.

For I_{21}-individuals: at each time step, there is a probability β_2 of being cured and becoming a R-individual. If this I_{21}-individual remains sick, there is a probability γ_2 of dying due to disease-2. These processes of recovery and death are represented by Eqs. (10) and (15), respectively.

For I-individuals: at each time step, there is a probability β of being cured and becoming a R-individual. If this I-individual remains sick, there is a probability γ of dying due to disease-2. These processes of recovery and death are represented by Eqs. (11) and (16), respectively.

For R-individuals: at each time step, there is a probability d of dying. This process of death is represented by Eq. (19).

Throughout a computational simulation, the health states of the N individuals are simultaneously updated in the end of each time step. Similar models based on PCA were already employed in epidemiological studies (Chaves and Monteiro, 2017; Ferraz and Monteiro, 2019; Monteiro et al., 2006; 2020a; Pereira and Schimit, 2018; Schimit and

Monteiro, 2009; Silva and Monteiro, 2014). Fig. 1 shows a pictorial representation of the model proposed in this work.

There are 20 positive constants in this model: k_1, k_2, k_3, k_4, k_5, b_1, b_2, β_1, β_2, β, c_1, c_2, γ_1, γ_2, γ, d_1, d_2, d, δ, and ν. It is infeasible to fully determine how each of these 20 parameters affects the dynamical behavior of 10 variables, which are the numbers of individuals in each health state. Observe that the immunosuppression caused by disease-1 corresponds to $\beta_2 < \beta$ (the recovery probability of I_{21} is lower than the recovery probability of I) and $\gamma_2 > \gamma$ (the death probability of I_{21} is greater than the death probability of I). By defining $B \equiv \beta/\beta_2$ and $G \equiv \gamma_2/\gamma$, a compromised immunity after infection by disease-1 corresponds to $B > 1$ and $G > 1$. Therefore, the greater the immunosuppression, the higher the values of B and G.

In this work, the influences of B and G are evaluated. Also, the minimum vaccination probability, denoted by ν_m, for eradicating disease-1 is determined in function of B and G for two lattice sizes n. These results are described in the next section.

3. Numerical results

Here, 17 of the 20 parameters are kept fixed. In the simulations, $k_1 = k_2 = k_3 = k_4 = k_5 = 1$ (thus, the infectiousness is the same for both diseases for S, R_1, R_2, and V-individuals), $b_1 = b_2 = \beta_1 = \beta = 30\%$ (thus, the recovery rate is the same for I_1, I_2, I_{12}, and I-individuals), $c_1 = c_2 = \gamma_1 = \gamma = 20\%$ (thus, the death rate is the same for I_1, I_2, I_{12}, and I-individuals), and $d_1 = d_2 = d = \delta = 10\%$ (thus, the death rate is the same for R_1, R_2, R, and V-individuals). Also, $n = 100$ (therefore, the host population is composed of 10,000 individuals) and the initial condition is $S(0)/N = 98\%$, $I_1(0)/N = 1\%$, and $I_2(0)/N = 1\%$. The parameters whose values are varied are β_2 (the recovery probability of I_{21}-individuals), γ_2 (the death probability of I_{21}-individuals), and ν (the vaccination probability of S-individuals).

Figs. 2 and 3 exhibit the time evolutions of the normalized infected subpopulations $I_1(t)/N$ (blue line), $I_2(t)/N$ (cyan line), $I_{12}(t)/N$ (green line), $I_{21}(t)/N$ (red line), and $I(t)/N$ (black line) for $\beta_2 = 30\%$ and $\gamma_2 = 20\%$. In Fig. 2, $\nu = 0\%$; in Fig. 3, $\nu = 10\%$. Since $\nu = 0\%$ in Fig. 2, disease-1 is equivalent to disease-2; hence, the time evolutions of $I_1(t)/N$ and $I_2(t)/N$ are similar, and the time evolutions of $I_{12}(t)/N$ and $I_{21}(t)/N$ are also similar. Obviously, in this figure, $I(t)/N = 0$. In Fig. 3, $\nu = 10\% > 0$; therefore, $I_1(t)/N$ tends to be below $I_2(t)/N$, and $I_{21}(t)/N$ tends to be below $I_{12}(t)/N$, because the vaccine reduces the numbers of individuals vulnerable to disease-1.

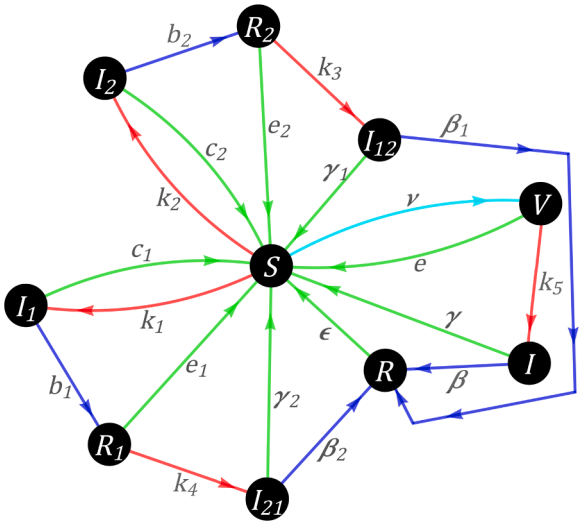

Fig. 1. Pictorial diagram of the proposed model. The 10 variables are inside the dark circles and the 20 parameters are near the lines representing the possible state transitions. Red lines are associated with contagion; blue lines with recovery; green lines with death, and cyan line with vaccination.

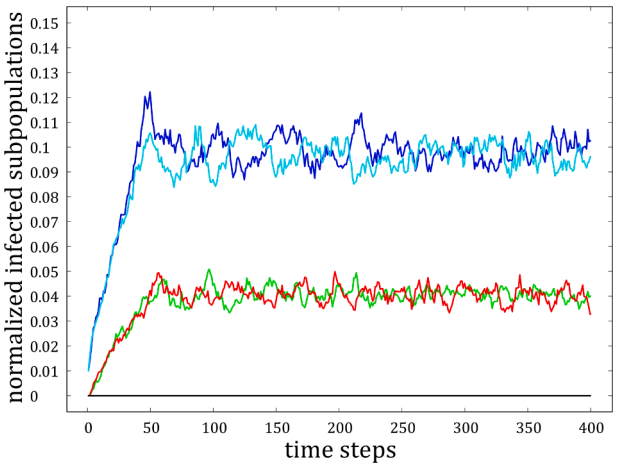

Fig. 2. Time evolutions of $I_1(t)/N$ (blue line), $I_2(t)/N$ (cyan line), $I_{12}(t)/N$ (green line), $I_{21}(t)/N$ (red line), and $I(t)/N$ (black line) from the initial condition $S(0)/N = 98\%$, $I_1(0)/N = 1\%$, and $I_2(0)/N = 1\%$. In this simulation, $n = 100$, $k_1 = k_2 = k_3 = k_4 = k_5 = 1$, $b_1 = b_2 = \beta_1 = \beta_2 = \beta = 30\%$, $c_1 = c_2 = \gamma_1 = \gamma_2 = \gamma = 20\%$, and $d_1 = d_2 = d = \delta = 10\%$. Also, $\nu = 0\%$. Note that $I_1(t)/N \to I_1^*/N \simeq 0.098$, $I_2(t)/N \to I_2^*/N \simeq 0.098$, $I_{12}(t)/N \to I_{12}^*/N \simeq 0.041$, $I_{21}(t)/N \to I_{21}^*/N \simeq 0.041$, and $I(t)/N = 0$.

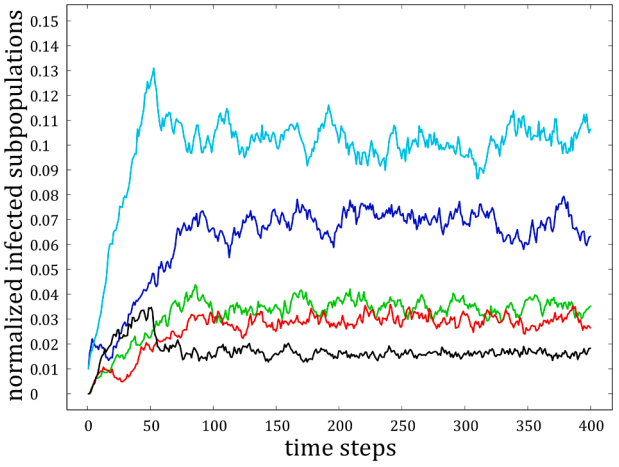

Fig. 3. Time evolutions of $I_1(t)/N$ (blue line), $I_2(t)/N$ (cyan line), $I_{12}(t)/N$ (green line), $I_{21}(t)/N$ (red line), and $I(t)/N$ (black line) for $\nu = 10\%$. The other parameter values are the same as those of Fig. 2. Note that $I_1(t)/N \to I_1^*/N \simeq 0.070$, $I_2(t)/N \to I_2^*/N \simeq 0.101$, $I_{12}(t)/N \to I_{12}^*/N \simeq 0.035$, $I_{21}(t)/N \to I_{21}^*/N \simeq 0.030$, and $I(t)/N \to I^*/N \simeq 0.016$.

Note that, as time passes by, these plots tend to fluctuate around average values, which are denoted by I_1^*/N, I_2^*/N, I_{12}^*/N, I_{21}^*/N, and I^*/N. These constants are the normalized average amounts obtained in the last 200 time steps from a total of 400 time steps. In Fig. 2, $I_1^*/N \simeq 0.098$, $I_2^*/N \simeq 0.098$, $I_{12}^*/N \simeq 0.041$, $I_{21}^*/N \simeq 0.041$, and $I^*/N = 0$; in Fig. 3, $I_1^*/N \simeq 0.070$, $I_2^*/N \simeq 0.101$, $I_{12}^*/N \simeq 0.035$, $I_{21}^*/N \simeq 0.030$, and $I^*/N \simeq 0.016$. Let Y be the sum of these normalized amounts; that is, $Y \equiv (I_1^* + I_2^* + I_{12}^* + I_{21}^* + I^*)/N$. For $\nu = 0\%$, $Y \simeq 0.278$; for $\nu = 10\%$, $Y \simeq 0.252$; for $\nu = 20\%$, $Y \simeq 0.216$; for $\nu = 30\%$, $Y \simeq 0.176$. Therefore, vaccination reduces Y. Also, in Figs. 2 and 3, $n = 100$; however, for $n = 200$, the same results are obtained. In fact, these normalized amounts do not depend on the lattice size n.

Figs. 4 and 5 show how B and G affect the numbers of infected individuals and the numbers of deaths due to both diseases for two values of ν. In these figures, $Y_1 = (I_1^* + I_{12}^*)/N$ and $Y_2 = (I_2^* + I_{21}^* + I^*)/N$; that is, Y_1 is the normalized number of individuals infected by disease-1 and

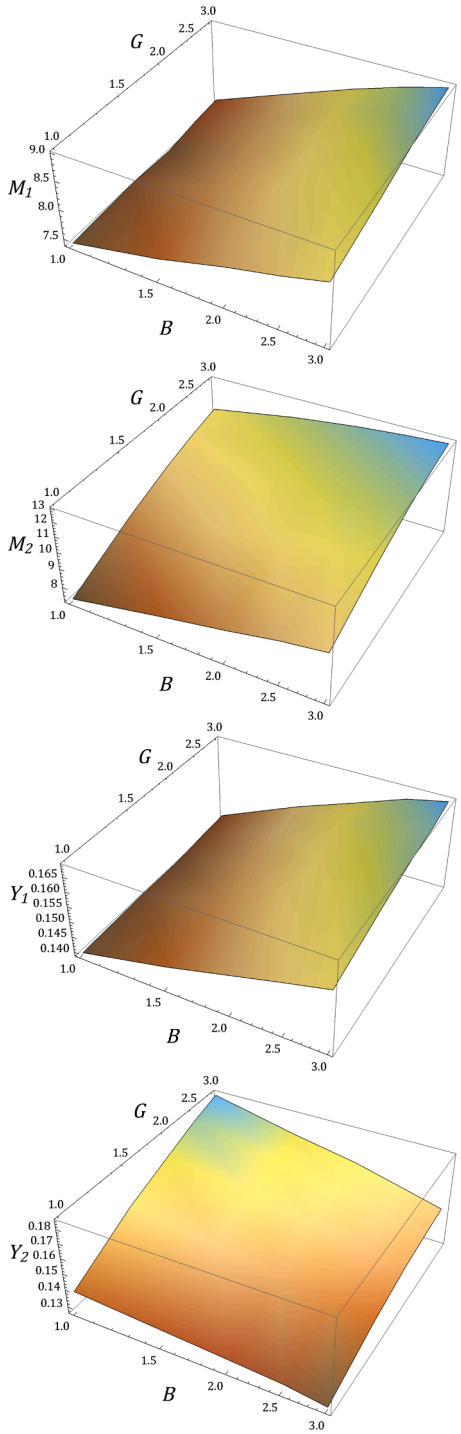

Fig. 4. Plots of three-dimensional surfaces of M_1, M_2, Y_1, and Y_2 in function of B and G, for $1 \leq B \leq 3$, $1 \leq G \leq 3$, and $\nu = 0\%$. The other parameter values are the same as those of Fig. 2.

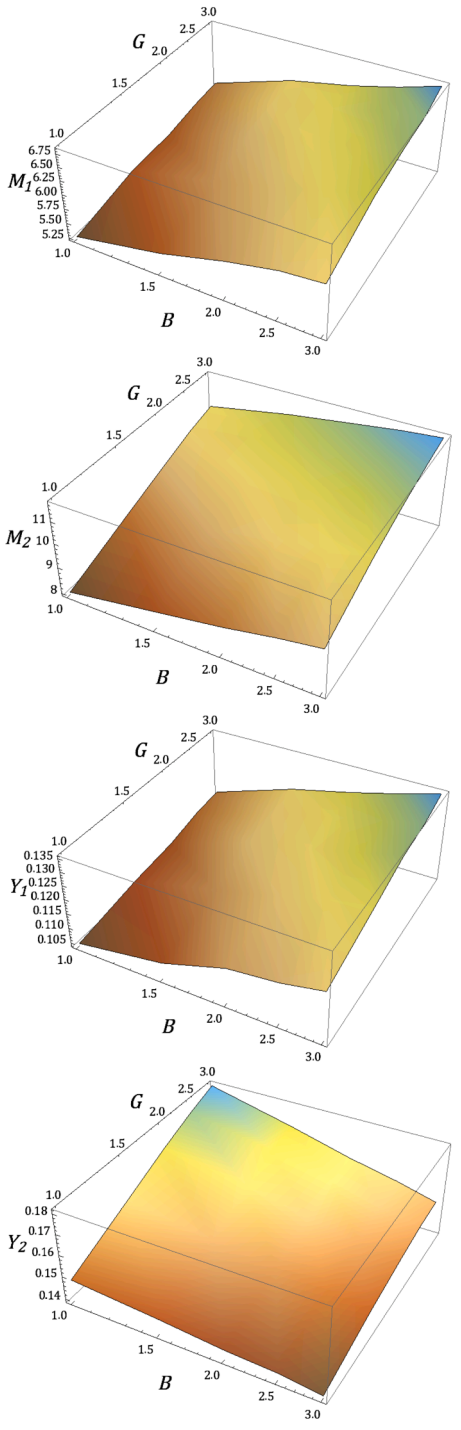

Fig. 5. Plots of three-dimensional surfaces of M_1, M_2, Y_1, and Y_2 in function of B and G, for $1 \leq B \leq 3$, $1 \leq G \leq 3$, and $\nu = 10\%$. The other parameter values are the same as those of Fig. 2.

Y_2 is the normalized number of individuals infected by disease-2, after the system reaching its endemic attractor. The variables M_1 and M_2 are the normalized numbers of deaths (the number of deaths divided by the population size N) caused by disease-1 and disease-2, respectively, during 400 time steps. Thus, M_1 and M_2 are related to mortality, and Y_1 and Y_2 to infection prevalence. These four variables are affected by the vaccination probability ν. Figs. 4 and 5 present average values of M_1, M_2, Y_1, and Y_2 obtained in three simulations. They reveal that Y_1, M_1, and M_2 increase with B and G; Y_2 decreases with B and increases with G.

The values of M_1, M_2, Y_1, and Y_2 in Fig. 4, for $\nu = 0\%$, are usually higher than the corresponding values in Fig. 5, for $\nu = 10\%$. For instance, for $B = 3$ and $G = 3$, $M_1 \simeq 9.0$, $M_2 \simeq 13$, $Y_1 \simeq 0.17$, and $Y_2 \simeq 0.15$ for $\nu = 0\%$; and $M_1 \simeq 6.8$, $M_2 \simeq 12$, $Y_1 \simeq 0.14$, and $Y_2 \simeq 0.15$ for $\nu = 10\%$.

Let respectively $y(\nu) \equiv Y(0) - Y(\nu)$ and $m(\nu) \equiv M(0) - M(\nu)$ be reductions due to vaccination $\nu > 0$ in the percentage of sick people and in the normalized cumulative deaths, as compared to the case $\nu = 0$. Recall that the variables $Y = Y_1 + Y_2$ and $M = M_1 + M_2$ vary with ν. From the numbers presented in the paragraph above, a vaccination probability of 10% against disease-1 saved $mN = [(9 + 13) - (6.8 + 12)] \times N = 32000$

lives of sick people in 400 time steps in a population of $N = 10000$ individuals, which corresponds to 80 lives (0.8% of the whole population) saved per time step. Also, the sick subpopulations were reduced in $y = [(0.17 + 0.15) - (0.14 + 0.15)] = 3\%$, which means 300 fewer sick individuals per time step.

Table 1 shows the values of y and m for $B = 3$ and $G = 3$ in lattices with $n = 100$ and $n = 200$. Note that y and m increase with ν and are not significantly affected by n. These results are valid for $\nu < \nu_m$.

Table 2 presents the minimum vaccination probability ν_m, for which disease-1 disappears in 5 consecutive simulations within the time window of 400 time steps, for $n = 100$ and $n = 200$. These minimum values were determined for $\{B, G\} = \{(1,1); (1,3); (3,1); (3,3)\}$, which are the corners of the surfaces shown in Figs. 4 and 5. Note that, the higher values of B and G, the higher the value of ν_m. This qualitative result is also obtained, for instance, for $d_1 = d_2 = d = \delta = 5\%$ (instead of 10%). In this case, for $n = 100$, $\nu_m = 11\%$ (instead of 33%) for $B = G = 1$ and $\nu_m = 14\%$ (instead of 43%) for $B = G = 3$. Reducing d_1, d_2, d, and δ means increasing the lifetime of immune individuals, which decreases the vaccination effort required to eradication because such reductions contribute to foster a herd immunity. Hence, ν_m decreases by reducing d_1, d_2, d, and δ.

The simulations reported here were performed with fictitious parameter values. However, realistic values for the proposed model can be obtained from real-world data by employing methods of parameter identification (see, for instance, Monteiro et al., 2020b).

Table 1
The values of $y = Y(0) - Y(\nu)$ and $m = M(0) - M(\nu)$ in function of ν for $n = 100$ and $n = 200$. Recall that y denotes the reduction in the percentage of sick individuals and mN is number of saved lives (thanks to vaccination) in 400 time steps. In this table, $B = 3$ and $G = 3$. The other parameter values are the same as those of Fig. 2.

ν	y for $n = 100$	m for $n = 100$	y for $n = 200$	m for $n = 200$
10%	0.03	3.2	0.03	3.3
20%	0.06	6.5	0.06	6.7
30%	0.11	10.6	0.12	10.5

Table 2
Minimum vaccination probability ν_m for eradicating disease-1 (in 5 consecutive simulations in a time window of 400 time steps) in function of B, G, and n. The other parameter values are the same as those of Fig. 2.

B	G	ν_m for $n = 100$	ν_m for $n = 200$
1	1	33%	35%
1	3	36%	40%
3	1	37%	42%
3	3	43%	43%

4. Discussion and conclusion

Recovery from measles confers long-life immunity to this viral infection; however, the post-recovery period is usually characterized by a significant and prolonged immunosuppression, which can last for years (Mina et al., 2019; Petrova et al., 2019). As a consequence, there is an increased incidence of secondary infections (Mina et al., 2019; Petrova et al., 2019). Vaccine against measles elicits long-lasting immunity without reducing the pre-acquired immunity to other pathogens. Therefore, this vaccine decreases not only the measles mortality, but also the mortality to subsequent non-measles infections (Mina, 2017; Rodrigues and Plotkin, 2020). In the proposed model, this vaccination effect is reproduced, because reductions in percentages of infected people and in cumulative deaths increase with ν, for $\nu < \nu_m$, as shown in Table 1 and Figs. 2–5.

Table 2 reveals that the higher the values of B and G, the higher the critical vaccination coverage ν_m to eradicate disease-1. In other words: the higher immunosuppression level caused by disease-1, the greater the efforts of public health agencies to encourage vaccination against this disease.

In the model, disease-1 can emulate the role of, for instance, measles or even COVID-19. In fact, COVID-19, in addition to causing respiratory problems, cerebrovascular disorders, neurological injuries, and psychological distress (Mahalakshmi et al., 2021), can also suppress host immunity (Remy et al., 2020), which can increase the vulnerability to future infections as measles does. In the model, disease-2 can be any non-vaccine preventable infection, such as hepatitis C, or a vaccine-preventable infection, but with poor adherence to vaccination, such as hepatitis A (Johnson et al., 2019).

In short, vaccination campaigns against measles/COVID-19 provide direct protection against measles/COVID-19 and also indirect benefits against other contagious diseases, by preserving the herd immunities of the host population. It is crucial that public health agencies undermine vaccine hesitancy and vaccine refusal. These are threats that can be treated by combating disinformation and fake news.

CRediT authorship contribution statement

G.F. Puga: Software, Validation, Formal analysis, Investigation, Resources, Data curation, Writing - original draft, Visualization, Funding acquisition. **L.H.A. Monteiro:** Conceptualization, Methodology, Validation, Formal analysis, Investigation, Resources, Writing - original draft, Writing - review & editing, Visualization, Supervision, Project administration, Funding acquisition.

Declaration of Competing Interest

The authors declare that they have no known competing financial interests or personal relationships that could have appeared to influence the work reported in this paper.

Acknowledgments

LHAM is partially supported by Conselho Nacional de Desenvolvimento Científico e Tecnológico (CNPq) under the grant #04081/2018-3. This study was financed in part by the Coordenação de Aperfeiçoamento de Pessoal de Nível Superior (CAPES) - finance code 001.

References

Ahmed, E., Agiza, H.N., Hassan, S.Z., 1998. On modeling hepatitis B transmission using cellular automata. J. Stat. Phys. 92, 707–712.
Alemneh, H.T., 2020. A co-infection model of dengue and leptospirosis diseases. Adv. Differ. Equ. 2020, 664.
Anggriani, N., Tasman, H., Ndii, M.Z., Supriatna, A.K., Soewono, E., Siregar, E., 2019. The effect of reinfection with the same serotype on dengue transmission dynamics. Appl. Math. Comp. 349, 62–80.
Boccara, N., Cheong, K., Oram, M., 1994. A probabilistic automata network epidemic model with births and deaths exhibiting cyclic behaviour. J. Phys. A: Math. Gen. 27, 1585–1597.
Chaves, L.L., Monteiro, L.H.A., 2017. Oscillations in an epidemiological model based on asynchronous probabilistic cellular automaton. Ecol. Complex. 31, 57–63.
Doran, J.R., Laffan, S.W., 2005. Simulating the spatial dynamics of foot and mouth disease outbreaks in feral pigs and livestock in Queensland, Australia, using a susceptible-infected-recovered cellular automata model. Prev. Vet. Med. 70, 133–152.
Ferraz, D.F., Monteiro, L.H.A., 2019. The impact of imported cases on the persistence of contagious diseases. Ecol. Complex. 40, 100788.
Ferreri, L., Venturino, E., 2013. Cellular automata for contact ecoepidemic processes in predator-prey systems. Ecol. Complex. 13, 8–20.
Johnson, K.D., Lu, X.Y., Zhang, D.M., 2019. Adherence to hepatitis A and hepatitis B multi-dose vaccination schedules among adults in the united kingdom: a retrospective cohort study. BMC Public Health 19, 404.
Mahalakshmi, A.M., Ray, B., Tuladhar, S., Bhat, A., Paneyala, S., Patteswari, D., Sakharkar, M.K., Hamdan, H., Ojcius, D.M., Bolla, S.R., Essa, M.M., Chidambaram, S. B., Qoronbfleh, M.W., 2021. Does COVID-19 contribute to development of neurological disease? Immun. Inflamm. Dis. 9, 48–58.
Mina, M.J., 2017. Measles, immune suppression and vaccination: direct and indirect nonspecific vaccine benefits. J. Infect. 74, S10–S17.

Mina, M.J., Kula, T., Leng, Y.M., Li, M.M., de Vries, R.D., Knip, M., Siljander, H., Rewers, M., Choy, D.F., Wilson, M.S., Larman, H.B., Nelson, A.N., Griffin, D.E., de Swart, R.L., Elledge, S.J., 2019. Measles virus infection diminishes preexisting antibodies that offer protection from other pathogens. Science 366, 599–606.
Monteiro, L.H.A., Chimara, H.D.B., Chaui Berlinck, J.G., 2006. Big cities: shelters for contagious diseases. Ecol. Model. 197, 258–262.
Monteiro, L.H.A., Fanti, V.C., Tessaro, A.S., 2020a. On the spread of SARS-CoV-2 under quarantine: a study based on probabilistic cellular automaton. Ecol. Complex. 44, 100879.
Monteiro, L.H.A., Gandini, D.M., Schimit, P.H.T., 2020b. The influence of immune individuals in disease spread evaluated by cellular automaton and genetic algorithm. Comput. Methods Programs Biomed. 196, 105707.
Moualeu, D.P., Mbang, J., Ndoundam, R., Bowong, S., 2011. Modeling and analysis of HIV and hepatitis C co-infections. J. Biol. Syst. 19.
Nagatani, T., Tainaka, K., 2018. Cellular automaton for migration in ecosystem: application of traffic model to a predator-prey system. Physica A 490, 803–807.
Pereira, F.M.M., Schimit, P.H.T., 2018. Dengue fever spreading based on probabilistic cellular automata with two lattices. Physica A 499, 75–87.
Petrova, V.N., Sawatsky, B., Han, A.X., Laksono, B.M., Walz, L., Parker, E., Pieper, K., Anderson, C.A., de Vries, R.D., Lanzavecchia, A., Kellam, P., von Messling, V., de Swart, R.L., Russell, C.A., 2019. Incomplete genetic reconstitution of B cell pools contributes to prolonged immunosuppression after measles. Sci. Immunol. 4, eaay6125.
Remy, K.E., Mazer, M., Striker, D.A., Ellebedy, A.H., Walton, A.H., Unsinger, J., Blood, T. M., Mudd, P.A., Yi, D.J., Mannion, D.A., 2020. Severe immunosuppression and not a cytokine storm characterizes COVID-19 infections. JCI Insight 5.E140329
Rodrigues, C.M.C., Plotkin, S.A., 2020. Impact of vaccines; health, economic and social perspectives. Front. Microbiol. 11, 1526.
Schimit, P.H.T., Monteiro, L.H.A., 2009. On the basic reproduction number and the topological properties of the contact network: an epidemiological study in mainly locally connected cellular automata. Ecol. Model. 220, 1034–1042.
Sfa, F.E., Nemiche, M., Rayd, H., 2020. A generic macroscopic cellular automata model for land use change: the case of the Dråa valley. Ecol. Complex. 43, 100851.
Silva, H.A.L.R., Monteiro, L.H.A., 2014. Self-sustained oscillations in epidemic models with infective immigrants. Ecol. Complex. 17, 40–45.
Slimi, R., El Yacoubi, S., Dumonteil, E., Gourbiere, S., 2009. A cellular automata model for chagas disease. Appl. Math. Model. 33, 1072–1085.
Tilahun, G.T., 2019. Modeling co-dynamics of pneumonia and meningitis diseases. Adv. Differ. Equ. 2019, 149.
Woolhouse, M.E.J., Gowtage-Sequeria, S., 2005. Host range and emerging and reemerging pathogens. Emerg. Infect. Dis. 11, 1842–1847.
Zhang, X.S., De Angelis, D., White, P.J., Charlett, A., Pebody, R.G., Mc Cauley, J., 2013. Co-circulation of influenza a virus strains and emergence of pandemic via reassortment: the role of cross-immunity. Epidemics 5, 20–33.